Available online at www.sciencedirect.com
ScienceDirect
International Journal of Pharmaceutics 353 (2008) 113–123
INTERNATIONAL JOURNAL OF PHARMACEUTICS
www.elsevier.com/locate/ijpharm

Experimental and computational morphology of three polymorphs of the free base of Venlafaxine: A comparison of morphology prediction methods

M.A. Deij [a,1], J. van Eupen [a,b], H. Meekes [a,*], P. Verwer [a,2], P. Bennema [b], E. Vlieg [a]

[a] *IMM Laboratory for Solid State Chemistry, Faculty of Science, Nijmegen University, Toernooiveld 1, NL-6525ED Nijmegen, The Netherlands*
[b] *Synthon BV, Microweg 22, NL-6545 CM Nijmegen, The Netherlands*

Received 8 May 2007; received in revised form 4 November 2007; accepted 13 November 2007
Available online 24 November 2007

Abstract

In this paper the experimental and the computational studies of the morphology of three polymorphs of the free base of Venlafaxine ((*N*,*N*-dimethyl)-2-(1-hydroxy cyclohex-1-yl)-2-(4-methoxyphenyl) ethylamine) are reported. The morphology of all polymorphs has been predicted using the Bravais–Friedel–Donnay–Harker method, the attachment energy method and kinetic Monte Carlo growth simulations and these predictions have been compared with experimental observations. The Monte Carlo simulations allow for a detailed simulation of the growth process, including driving force and growth mechanism, which leads to a semi-quantitative prediction of the growth morphologies of all three phases.

For phase **I** two distinct growth habits are found experimentally under the same conditions. This is explained by the occurrence of a spiral growth mechanism in one of the two, which was observed using AFM and which is also supported by the Monte Carlo simulations. The habit of phase **II** could only be explained from simulations when a spiral growth mechanism is assumed; the shape of phase **III** could not be modeled accurately from the Monte Carlo simulations. Although the shape of the crystal is reproduced accurately, some of the indices of the faces predicted are not in agreement with the indices measured. The deviations are interpreted to be due to the presence of domains in the crystals as a result of the layered structure.

Keywords: Crystal; Morphology prediction; Monte Carlo

1. Introduction

The study of polymorphism of pharmaceutical compounds is an important part in the development of a new drug (Vippagunta et al., 2001). As each polymorph has different metabolical characteristics, often only one polymorph can be used in a drug formulation (York, 1983). Knowledge of the polymorphs and their relative stabilities is therefore indispensable for the development of drugs that are administered in crystalline form. Apart from formulation issues, each new polymorph can be patented, so also for protection of intellectual property adequate knowledge of polymorphism is needed.

Polymorphs can have different crystal morphologies, because morphology is largely determined by the crystal packing at the molecular level and the crystallization process. It is desirable to be able to exert control over the morphology, because it determines among other things the bioavailability and the processability of the compound. The bioavailability depends on the dissolution rate of the crystals, which is in turn partly determined by the crystal morphology. Concerning processability, it can generally be said that block-like crystal habits are desired over plate-like crystals and needles because the latter forms tend to block filters, are more difficult to dry and give problems during tabletting.

Crystal morphology can be predicted computationally using various methods of different complexity and demand for computing power. Well-known approaches are the method developed by Bravais, Friedel, Donnay and Harker (BFDH) based on the interplanar distances of crystallographic orientations (Donnay and Harker, 1937, 1961) and the method developed by Hartman and Perdok (1955a,b,c), and later by Hartman and Bennema

* Corresponding author.
E-mail address: hugo.meekes@science.ru.nl (H. Meekes).
[1] Present address: Avantium Technologies BV, Department of Predictive Technologies, Zekeringstraat 29, 1014 BV Amsterdam, The Netherlands.
[2] Present address: Akzo Nobel Chemicals, Research and Technology Center, P.O. Box 9300, 6800 SB Arnhem, The Netherlands.

0378-5173/$ – see front matter © 2007 Elsevier B.V. All rights reserved.
doi:10.1016/j.ijpharm.2007.11.034

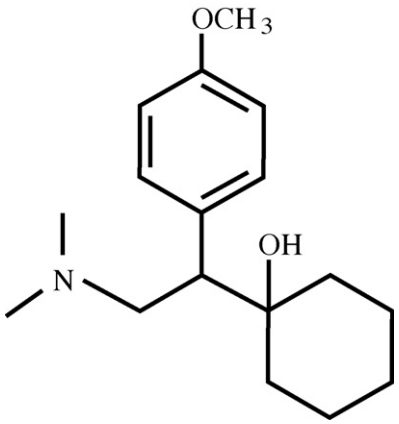

Fig. 1. Molecular structure of Venlafaxine.

(1980), which uses the concept of the crystal graph to determine the slice and attachment energies of crystallographic orientations, and relates these energies to the growth rate of the orientations.

The development of detailed crystal growth simulations, for instance using Monte Carlo techniques, has been facilitated by the ongoing development and availability of ever faster computers. A recent development is a program called MONTYwith which growth simulations can be performed for arbitrary crystal structures in any crystallographic orientation as a function of the driving force for crystallization (Boerrigter et al., 2004).

Here the results are presented of a morphology prediction study for the three polymorphs of Venlafaxine using all three methods. A comparison with the morphologies observed experimentally is made. It is found that the predictions are semi-quantitative for phases **I** and **II**; for phase **III** the overall shape is reproduced, but some predicted indices do not match the indices observed experimentally.

2. Venlafaxine

Venlafaxine is a bicyclic phenylethylamine-based antidepressive drug, which is believed to work by simultaneously blocking the re-uptake of neuronal norepinephrine and serotonin

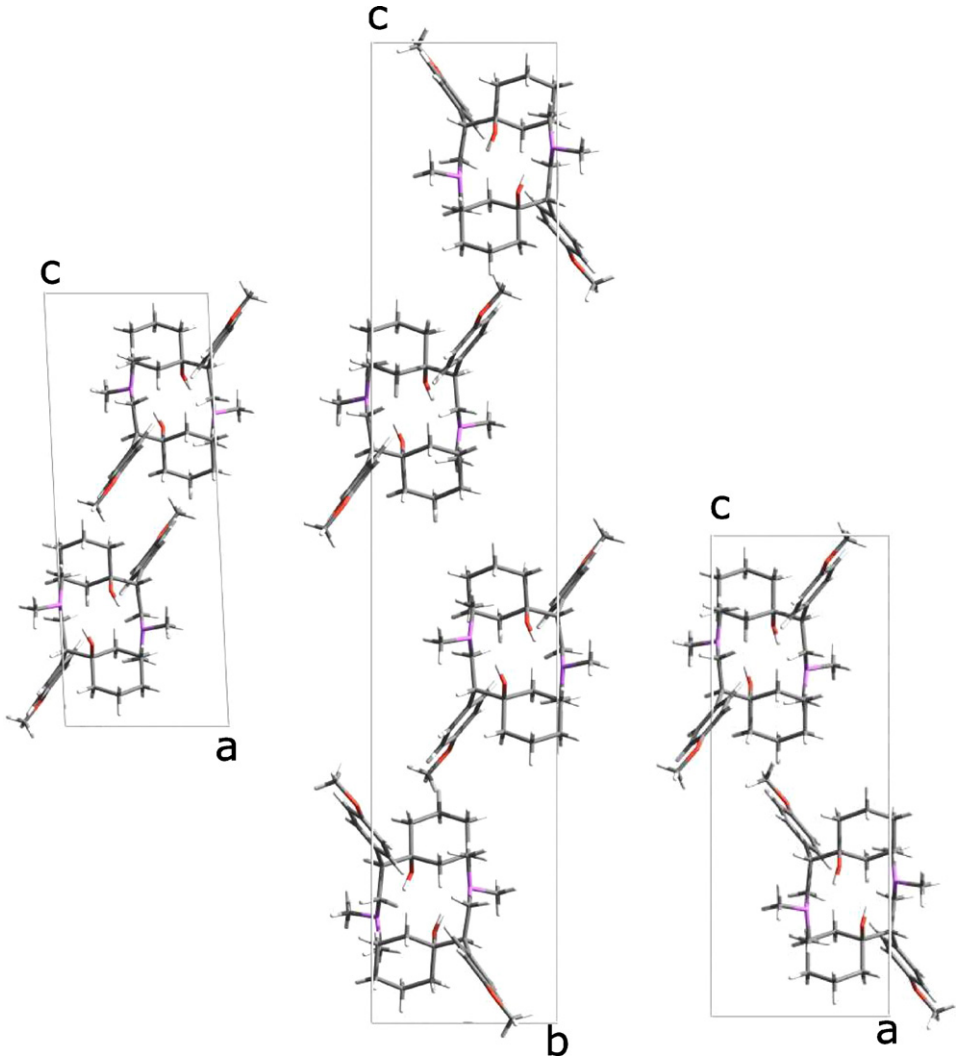

Fig. 2. Crystal structures of phase **I** (left), phase **II** (middle) and phase **III** (right). The packing similarities can be seen, conceptually, as phase **II** being built up of layers of phase **I** and **III**.

Table 1
Lattice parameters and energies of the three phases before and after geometry optimization

Structure	Space group	Z	a (Å)	b (Å)	c (Å)	β	Lattice energy (kcal mol^{-1})
Phase **I**	$P12_1/n1$	4	8.21	8.86	21.79	92.79	
—optimized							
			8.28	9.32	22.47	93.71	−28.6
Phase **II**	$P12_1/c1$	8	8.84	8.27	43.75	90.97	
—optimized							
			9.28	8.35	44.63	92.41	−28.9
Phase **III**	$P2_12_12_1$	4	8.22	8.86	22.27	90.00	
—optimized							
			8.25	9.27	22.74	90.00	−28.8

(Husbands et al., 1987). The Venlafaxine molecular structure is shown in Fig. 1. It is administered as a racemic mixture, and the crystals of this mixture are the subject of this study. Recently it has been found that the free base of Venlafaxine has superior processing characteristics over the hydrochloric acid salt, which is marketed worldwide. The free base is easier to handle as it is less aggressive towards equipment etc. compared to the hydrochloric acid salt. Also, the free base shows a low solubility and low dissolution rate in water, and is therefore suitable for the formulation of extended release dosage forms (Picha et al., 2003). In the study of the free base, three polymorphs have been found, which are enantiotropically related (van Eupen et al., 2008). Phase **I** is stable at room temperature, and can be converted into phase **II** above approximately 40 °C. Phases **I** and **II** can be converted into phase **III** above 60 °C.

It can be seen from Fig. 2 that the crystal structures (van Eupen et al., 2008) of the three polymorphs are strongly related. When viewed along the **b**-axis, the unit cell of phase **I** consists of four molecules whose methoxyphenyl rings are oriented in a parallel fashion. In the crystal structure of phase **III**, the molecules stack with the methoxyphenyl rings in mutually perpendicular orientation. In the crystal structure of phase **II** these patterns of phases **I** and **III** are both incorporated; phase **II** can be thought of to be built of {0 0 2} layers of phases **I** and **III**. It must be noted, however, that this comparison only holds at a conceptual level, as due to packing details the crystal structures can not be overlaid exactly.

Thus all polymorphs are built up of two types of layers, and each layer consists of enantiopure molecules (*R* or *S*). The polymorphs differ in the way that the *R* and *S* layers are stacked. Phases **I** and **II** are racemates, having space group $P2_1/n$ and $P2_1/c$, respectively. Phase **I** stacks with alternating *R* and *S* layers; phase **II** with two *R* layers followed by two *S* layers.

Interestingly, phase **III** has space group $P2_12_12_1$, a chiral space group. Phase **III** can, however, be obtained from racemic solutions. It was shown using enantiomeric etch experiments (van Eupen et al., 2008), that phase **III** is a conglomerate, built up of enantiopure macroscopic *R* and *S* layers: upon immersion of a crystal of phase **III** in a supersaturated solution of one enantiomer, the other enantiomer is etched away, and μm-thick layers of enantiopure material are left. The enantiomeric enrichment of the remaining solid was proven by determination of the optical rotation of a crystal dissolved after etching.

As all polymorphs are enantiotropically related, the solid state conversion of phases **I** and **II** to phase **III** at higher temperatures is very remarkable, as that implies large movements of molecules from a molecularly racemic configuration to an enantiomeric conglomerate. Still, the etch experiments showed that a crystal that had been transformed from phases **I** to **III** is indeed a conglomerate of enantiopure material. For further

Table 2
Crystal graph bonds for the three phases of Venlafaxine

Phase **I**			Phase **II**			Phase **III**		
Bond	Unscaled	Scaled	Bond	Unscaled	Scaled	Bond	Unscaled	Scaled
1–2 [0 0 0]	−7.81	−3.20	1–8 [1 0 0]	−8.13	−5.44	1–3 [0 0 0]	−7.59	−4.02
1–3 [0 1 0]	−5.98	−2.45	1–8 [0 0 0]	−7.58	−5.07	1–3 [1 0 0]	−4.55	−2.41
1–2 [1 0 0]	−4.64	−1.90	1–5 [1 0 $\bar{1}$]	−5.83	−3.90	1–4 [0 $\bar{1}$ 1]	−3.84	−2.04
1–3 [0 0 0]	−3.98	−1.63	1–5 [0 0 $\bar{1}$]	−4.78	−3.19	1–1 [$\bar{1}$ 0 0]	−3.50	−1.85
1–1 [$\bar{1}$ 0 0]	−3.58	−1.47	1–8 [1 1 0]	−4.54	−3.04	1–1 [0 $\bar{1}$ 0]	−2.70	−1.43
1–1 [0 $\bar{1}$ 0]	−2.58	−1.05	1–8 [0 1 0]	−4.52	−3.02	1–4 [0 0 1]	−2.69	−1.42
1–3 [$\bar{1}$ 0 0]	−1.67	−0.68	1–1 [0 $\bar{1}$ 0]	−3.49	−2.34			
			1–1 [$\bar{1}$ 0 0]	−2.54	−1.70			
			1–5 [0 $\bar{1}$ $\bar{1}$]	−1.60	−1.07			
			2–4 [0 $\bar{1}$ 0]	−4.00	−2.67			
			2–2 [0 $\bar{1}$ 0]	−3.20	−2.14			
			2–4 [$\bar{1}$ $\bar{1}$ 0]	−2.75	−1.84			
			2–2 [$\bar{1}$ 0 0]	−2.72	−1.82			

In the first column the bond offset is listed, in the second the bond strength in kcal mol^{-1}. For example, the first line indicates a bond going from GU 1 to GU 2 in the same unit cell. This bond has an unscaled strength of −7.81 kcal mol^{-1} and a scaled bond strength of −3.20 kcal mol^{-1}. Bonds that are related by symmetry are not listed.

details, the reader is referred to reference van Eupen et al. (2008).

3. Morphology prediction

Generally speaking, growth morphologies can be constructed using a kinetic Wulff construction. In this construction the distance $\mathbf{r}_{h\,k\,l}$ of a face $(h\,k\,l)$ from the origin of the crystal is taken to be linearly related to the growth rate $R_{h\,k\,l}$ of that face:

$$\mathbf{r}_{h\,k\,l} \propto R_{h\,k\,l} \tag{1}$$

By constructing a three-dimensional set of faces perpendicular to the crystallographic orientations $(h\,k\,l)$ the growth morphology can be constructed if the growth rates of the faces are known. Different theories have been developed to derive or compute expressions for the growth rate $R_{h\,k\,l}$. Three of these will be discussed below.

3.1. BFDH method

Although being an approach for predicting equilibrium morphology, the BFDH method is commonly used to relate the growth rate of a crystallographic orientation to the inverse of the interplanar distance $d_{h\,k\,l}$. The relevant indices $(h\,k\,l)$ are those allowed by the space group selection rules. The distance from the center of the crystal to a surface $(h\,k\,l)$ is then given by

$$|\mathbf{r}_{h\,k\,l}| = \frac{1}{d_{h\,k\,l}}. \tag{2}$$

In retrospect, the rationale behind the method is that the larger $d_{h\,k\,l}$ is, the larger the energy content of the growth layer will be, and therefore the smaller the growth rate of the corresponding orientation will be. This limits the predictive power of the BFDH method in the case of anisotropic crystal structures. The determination of the values for $d_{h\,k\,l}$, however, is trivial once the space group and lattice parameters are known, making BFDH a very fast method.

3.2. Hartman–Perdok theory and the determination of the crystal graph

In the extension of the Hartman–Perdok theory by Hartman and Bennema, the concept of the crystal graph is introduced (Hartman and Bennema, 1980). The crystal graph is a mathematical representation of the crystal structure as an infinite three-dimensional graph, in which the graph vertices represent the growth units and the graph edges represent the interactions between the growth units.

The crystal graph is used to determine Periodic Bond Chains (PBCs). PBCs are uninterrupted chains of bonds between symmetry-related growth units with an overall periodicity $[uvw] = u\mathbf{a} + v\mathbf{b} + w\mathbf{c}$, $(u, v, w \in \mathbb{Z})$ of the primitive lattice, which contains no other lattice translation. PBCs are stoichiometric with respect to the contents of the crystal unit cell. Combinations of two or more intersecting PBCs in non-parallel directions in a growth layer define so-called connected nets.

Crystallographic orientations that have connected nets are likely to determine the growth morphology of the crystal (Grimbergen et al., 1998). In the Hartman–Perdok theory, the attachment energies of the connected nets in all crystallographic orientations determine the growth morphology. The bonds that are present in a crystal slice together make up the crystal's slice energy; the other bonds define the slice attachment energy. Together, they are equal to the crystallization energy:

$$\begin{aligned} E^{\mathrm{att}}_{h\,k\,l} &= \sum_i \phi^{i,\mathrm{att}}_{h\,k\,l} \\ E^{\mathrm{slice}}_{h\,k\,l} &= \sum_i \phi^{i,\mathrm{slice}}_{h\,k\,l} \\ E^{\mathrm{cryst}} &= E^{\mathrm{att}}_{h\,k\,l} + E^{\mathrm{slice}}_{h\,k\,l} \end{aligned} \tag{3}$$

Once the attachment energies for all orientations that have one or more connected nets have been computed, the attachment energies are related to growth rates $R_{h\,k\,l}$ as

$$R_{h\,k\,l} \propto E^{\mathrm{att}}_{h\,k\,l} = E^{\mathrm{cryst}} - E^{\mathrm{slice}}_{h\,k\,l} \tag{4}$$

allowing for the prediction of the attachment energy morphology. The attachment energy method can thus be considered as a refinement of the BFDH method using the slice energy as the parameter determining the growth. The BFDH method uses the interplanar distance, which is merely a geometrical parameter.

3.3. Monte Carlo growth simulations

The methods described above give a reasonable approximation of the growth morphology in several cases. It is well-known, however, that the growth morphology depends on the driving force (i.e. the solution supersaturation) and growth mechanism during growth of the crystal (van der Eerden, 1993). This is not taken into account when a morphology is calculated using the BFDH approach nor when based on the Hartman–Perdok theory. Recently the program MONTY was developed by Boerrigter et al. that is able to perform growth simulations on any crystal structure in any crystallographic orientation (Boerrigter et al., 2004).

In these simulations a box with lateral periodic boundary conditions is prepared in a certain crystallographic orientation $(h\,k\,l)$ on which particles may attach and detach with the following probabilities:

$$\begin{aligned} \mathcal{P}^{+}_{ij} &= \exp(-\beta\lambda(\Delta U - \Delta U_{ij}) - \beta(\lambda - 1)(\Delta\mu)) \\ \mathcal{P}^{-}_{ij} &= \exp(-\beta(\lambda - 1)(\Delta U - \Delta U_{ij}) - \beta\lambda(\Delta\mu)) \end{aligned} \tag{5}$$

where ij denotes a particle i having a bonding configuration j with surface bonding energy U_{ij} and $\beta = (k_{\mathrm{B}}T)^{-1}$. These probabilities ensure microscopic reversability at all times. The probabilities allow for a choice of the parameter $0 \le \lambda \le 1$, which controls the contribution of $\Delta\mu$ vs. the surface bonding ΔU_{ij} to the probabilities. When $\lambda = 0$, the attachment probability, $\mathcal{P}^{+}_{ij}$ is completely determined by the driving force $\Delta\mu$ and the detachment probability $\mathcal{P}^{-}_{ij}$ is completely determined by the surface bonding energy ΔU_{ij}. This probability scheme is called 'random rain' and has been shown to give good results for the

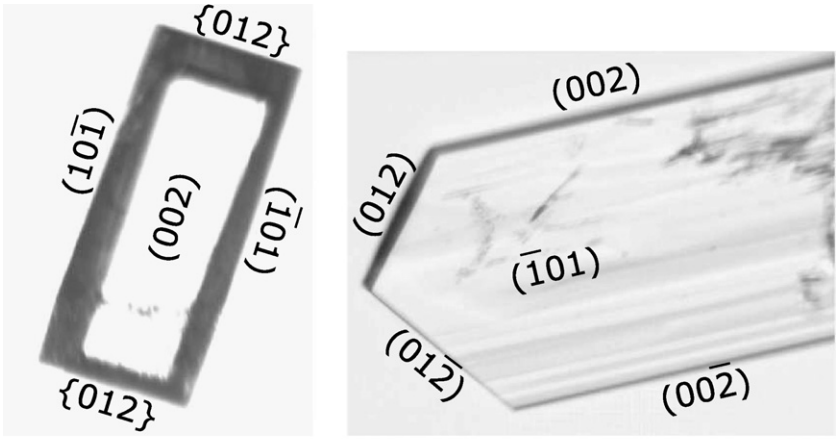

Fig. 3. Experimental habits of phase **I** grown from heptane solution. (a) shows the rectangular morphology without a spiral pattern on {0 0 2}, (b) shows the morphology with a spiral growth mechanism on {0 0 2}, leading to a more plank-like morphology with relatively large {$\bar{1}$ 0 1}faces.

simulation of crystal growth from solution (Cuppen et al., 2003). This is the probability scheme used for all growth simulations in this paper, as the Venlafaxine crystals are obtained from a heptane solution. Growth rates can be computed directly from the Monte Carlo results, allowing for a kinetic Wulff construction of the growth morphology.

4. Computational methods

4.1. Calculation of the crystal graphs

The crystal graphs were calculated using crystal structures obtained from single crystal X-ray diffraction (van Eupen et al., 2008). The geometries of the molecular conformations from the experimental structures were optimized using Gaussian 94 with an HF/6-31G* basis set (Frisch et al., 1995). A self-consistent field (SCF) convergence criterion of 10^{-8} as well as a "Tight" minimization threshold was applied. Charges were fitted to the nuclei using a restricted electrostatic potential (RESP) charge fitting scheme (Cornell et al., 1993). This RESP procedure serves two goals: first of all, it is known that RESP charges are less sensitive to small perturbations in the geometry, that will happen when the crystal structure is minimized (*vide infra*). Secondly, the RESP procedure was applied to all polymorph conformers at the same time, in order to obtain a single charge set that describes all molecular electrostatic potentials. In this way lattice energies of the two polymorphs can be compared directly, instead of having to calculate, estimate or ignore the cost in energy for changing the charge distribution going from one conformation to the other. This procedure is based on the R.E.D. v1.0 procedure developed by Pigache et al. (Pigache et al., 2004).

The molecular structures thus obtained were used to build the crystal structures, which were consecutively minimized using the Dreiding force field (Mayo et al., 1990) and the "Smart Minimizer" of Cerius^2(Cerius, 1997), with Ewald sums for the van der Waals and Coulomb contributions and high convergence settings.

Pairwise interactions were calculated using the Dreiding forcefield in the Cerius^2 program using a direct calculation of van der Waals and Coulomb contributions with a constant ϵ_r value. In contrast, the default value of ϵ_r in the Cerius^2 implementation of the Dreiding forcefield scales linearly with the distance, to approximate solvent effects (Mayo et al., 1990). Crystal graphs were created from all pairwise interactions up to a certain cutoff radius. The resulting interactions were then scaled so that their sum was equal to the dissolution enthalpy in heptane of each polymorph. Any scaled interactions with bond strength below a certain cutoff-value (usually kT) were discarded.

4.2. Attachment energy calculations

Once the energies of the bonds making up the crystal graph have been determined, attachment energies can be calculated from the crystal graph by the program FACELIFT (Grimbergen et al., 2006). This program finds all PBCs in the graph and subsequently combines them to form connected nets. The bonds that make up the connected net are the slice bonds; the bonds that attach connected nets to each other are the attachment energy bonds. The FACELIFT routine is also implemented in the Hartman–Perdok module of Cerius^2 (Cerius, 1997).

4.3. Monte Carlo simulations

The MONTY simulations were performed on surfaces ($h\,k\,l$) for which a connected net was found using the FACELIFT program. All simulations were performed on a rectangular grid of unit cells parallel to the orientation ($h\,k\,l$). For all orientations a simulation box of 50 × 50 unit cells with lateral periodic boundary conditions was used. The sampling in the simulations was preceded by a period of relaxation, in which the surface was allowed to grow under the same driving force as during

the simulation. This relaxation time was taken to be 100,000 events in all simulations. The sampling to determine the growth rate was subsequently done at least 500 times, with periods of 10,000 events in between. When there was reason to believe that the simulations needed more sampling time, as judged from the development of height vs. number of events, the sampling time was increased to a maximum of 10,000 sampling events all with 10,000 moves in between. In order to prevent long equilibration times at low driving forces, the simulations were performed on the same surface for decreasing driving force, i.e. the final surface configurations at higher $\Delta\mu/kT$ were used as the initial surface configuration for simulations at lower values.

5. Results and discussion

5.1. Crystal graph calculation

Using the methods outlined above, the energies of the crystal structures were minimized using a single charge set for all conformers of the three polymorphs. The resulting lattice parameters and lattice energies are listed in Table 1. The lattice energies are very close, and given the error associated with the force field, no stability ranking can be made on the basis of these energies. The similarity of the crystal structures, as shown in Fig. 2, is reflected in the fact that these lattice energies are so close. Next, all pairwise interactions were calculated. For all phases the unscaled interactions below -1.5 kcal mol^{-1}were used. The included bonds were subsequently scaled to the dissolution enthalpy.

This procedure resulted in crystal graphs in which the total number of bonds between the growth units is equal to 11 for phase **I** and 12 for phases **II** and **III**. The bonds not related by symmetry are listed in Table 2. It must be noted that for phase **II** the maximum number of bonds listed in this table does not correspond to the total number of bonds between growth units, as some bonds are not present for all growth units. This is due to the fact that for this phase, the number of growth units in the asymmetric unit cell, Z', is equal to 2.

5.2. Experimentally observed habits

Phase **I** exhibits two distinct morphologies, both displayed in Fig. 3. The ($h\,k\,l$) indices were determined using an optical goniometer. Both morphologies have the faces {0 0 2}, {1 0 $\bar{1}$} and {0 1 2}, one has {0 0 2} as the largest faces (Fig. 3a), the other has {1 0 $\bar{1}$} as the largest faces (Fig. 3b). The difference between the two habits is attributed to the presence of a dislocation on the {0 0 2} face leading to a spiral growth mechanism for the crystals shown in Fig. 3b. The presence of the typical spiral growth pattern on the {0 0 2} surface was confirmed experimentally using Differential Interference Contrast Microscopy (DICM) for the crystals having the morphology of Fig. 3b and no spirals were found on the {0 0 2} surface of the crystals having the morphology displayed in Fig. 3a. These microscopy images are displayed in Fig. 4.

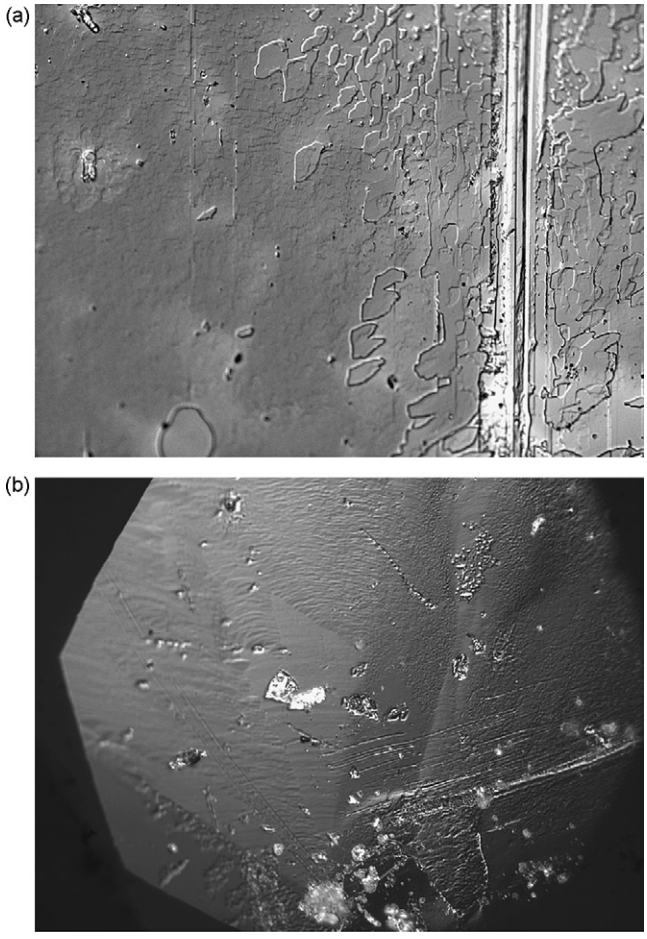

Fig. 4. Differential interference contrast microscopy (DICM) images of phase **I** shows (a) the presence of 2D islands and (b) spiral growth hillocks. The magnification factor is 200 ×. These micrographs were taken of the {0 0 2} surface for samples corresponding to the two different morphologies as displayed in Fig. 3.

The indices of the experimental habit of phase **II** could not be determined using the optical goniometer, so the experimental habit, shown in Fig. 5, has no indices. Still, it can be seen that also this phase has a plank-like shape, with similar top faces as phase **I**. The crystals of phase **II** consist of domains parallel to the basal face, which is, very likely, {0 0 2} (*vide infra*). These domains were found using a polarization microscope as alternating extinct and bright striped patterns on the side faces, depending on the orientation of the crossed polarizers. These domains were interpreted as twin domains typical for the monoclinic space group $P12_1/c1$ of this phase in combination with its layered crystal structure (see Fig. 2). As a result we can conclude that the basal face is {0 0 2} and the **b**-axis is parallel to the long axis of the crystals. The presence of these domains and the corresponding domain walls gives rise to a lot of macrosteps and striations on the side and top faces, as can be seen in the lower image of Fig. 5. Such striations can act as sources for growth steps leading to vicinal orientations. This explains the problem with indexing the habit of phase **II**.

The experimental habit of phase **III** is also a flat plank-like shape, displayed in Fig. 6. The indices are {0 0 2} (the basal face), {1 0 1} (side faces) and {0 1 2} (top face).

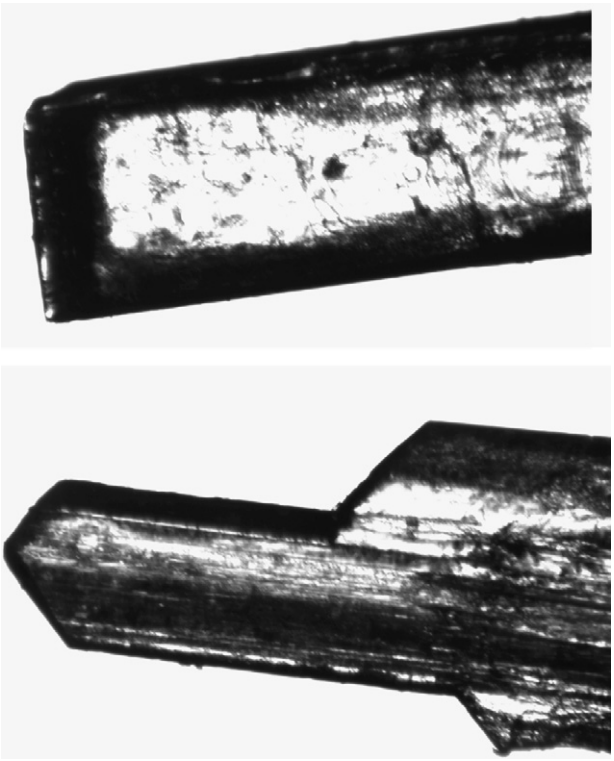

Fig. 5. Experimental habit phase **II** grown from heptane solution. This habit could not be indexed on a goniometer, so no indices are given.

5.3. Prediction of morphologies

5.3.1. BFDH

The morphologies were first predicted using the BFDH theory. The results for the three phases of Venlafaxine are displayed in Fig. 7. As can be seen in these figures, the predicted morphologies of phase **I** and **III** are very similar, due to the fact that the lattice parameters are quite similar. Differences are mainly caused by the difference in space group, $P2_1/c$ for phase **I** and $P2_12_12_1$ for phase **III**. As the unit cell of phase **II** has a **c**-axis that is about twice as long as the **c**-axes of phases **I** and **III**, the predicted shape of phase **II** is more plate-like. None of the predictions of the BDFH theory are very good however, as square shapes are predicted, instead of the experimentally

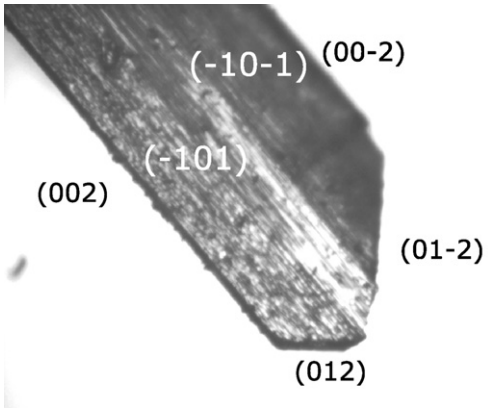

Fig. 6. Experimental habit phase **III** grown from heptane solution.

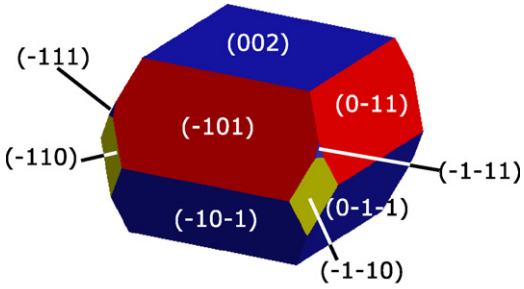

(a) BFDH morphology of phase I.

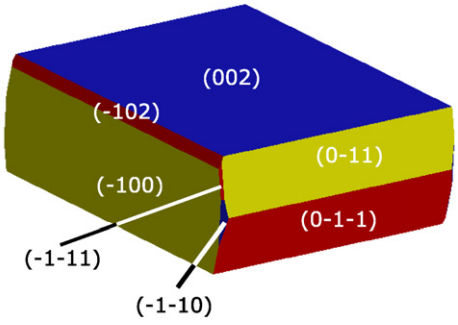

(b) BFDH morphology of phase II.

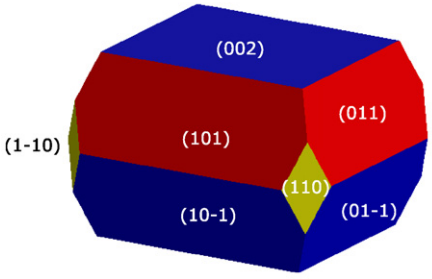

(c) BFDH morphology of phase III.

Fig. 7. The BFDH morphologies of the three phases of Venlafaxine.

observed plank-like morphologies. Also, for phases **I** and **III**, the predicted shapes are too thick in the {0 0 2} orientations.

5.3.2. Attachment energies

For phase **I** the FACELIFT procedure results in a set of 170 PBCs and 63 connected nets in 13 crystallographic forms; for phase **II** however, these numbers are much higher because of the larger number of particles in the unit cell. For phase **II** 36,922 PBCs and 4427 connected nets in 25 crystallographic forms were found. For phase **III**, 288 PBCs were found which could be combined to form 57 connected nets in 9 crystallographic forms.

The connected net attachment energies of phases **I**, **II** and **III** are shown in Table 3. The predicted morphologies obtained from these data are shown in Fig. 8. This prediction is much better than that of the BFDH method; for phase **I**, the {0 0 2}

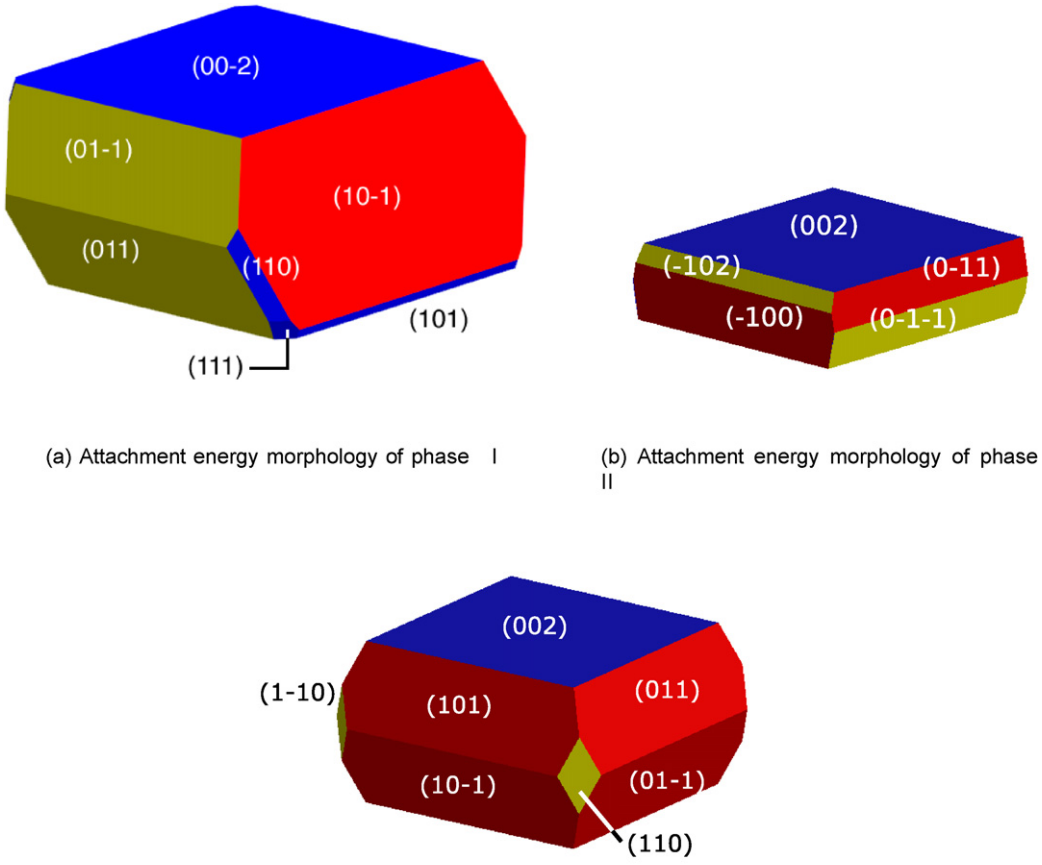

Fig. 8. The attachment energy morphologies of the three phases of Venlafaxine.

and $\{1\,0\,\bar{1}\}$ orientations are both predicted correctly. The attachment energy of the $\{0\,1\,1\}$ orientation is very close to that of $\{0\,1\,2\}$ orientation, so the former is favored over the latter in the predicted morphology. The observed rectangular plank-like morphology is not reproduced, however, as the predicted morphology is almost square. Phase **II** also has an almost square attachment energy morphology, and orientations $\{0\,0\,2\}$, $\{1\,0\,0\}$, $\{\bar{1}\,0\,2\}$ and $\{0\,1\,1\}$ are predicted. The third phase has the orientations $\{0\,0\,2\}$, $\{1\,0\,1\}$ and $\{0\,1\,1\}$ correctly predicted, and $\{1\,1\,0\}$ predicted but not observed. The general shape is too thick and square, as opposed to the elongated plank-like shape of phase **III**, observed experimentally.

5.3.3. *Monte Carlo growth simulations*

The growth rates of all connected net orientations of phase **I** as a function of the relative driving force $\Delta\mu/kT$ are dis-

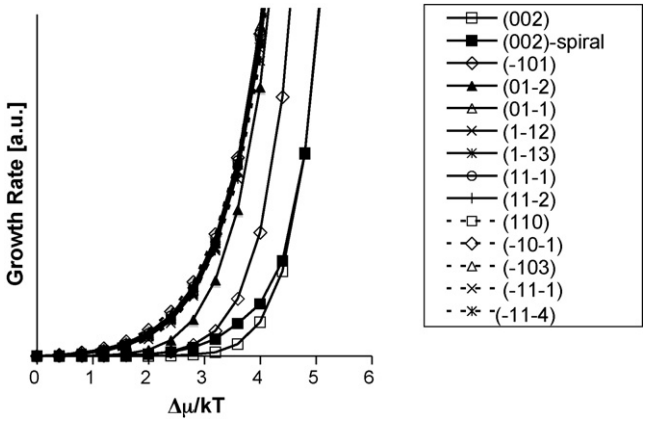

Fig. 9. Monte Carlo growth rate simulations for phase **I**.

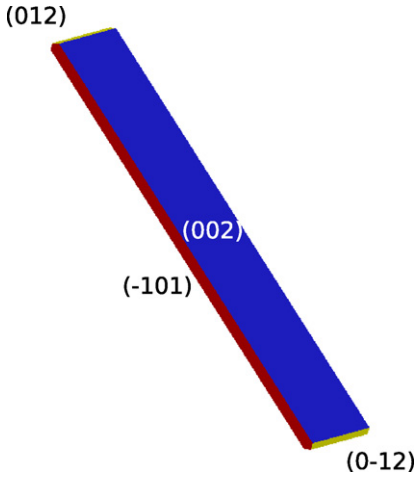

Fig. 10. Predicted morphology for phase **I** at $\Delta\mu/kT = 2.4$.

Table 3
F-faces and corresponding attachment energies of the three phases of Venlafaxine

Phase **I**		Phase **II**		Phase **III**	
$(h\,k\,l)$	E_{att} (kcal mol^{-1})	$(h\,k\,l)$	E_{att} (kcal mol^{-1})	$(h\,k\,l)$	E_{att} (kcal mol^{-1})
{0 0 2}	−23.25	{0 0 $\bar{2}$}	−24.41	{0 0 $\bar{2}$}	−26.14
{$\bar{1}$ 0 1}	−36.21	{0 $\bar{1}$ $\bar{1}$}	−79.73	{$\bar{1}$ 0 $\bar{1}$}	−45.25
{0 1 $\bar{1}$}	−46.50	{0 1 2}	−86.38	{0 1 $\bar{1}$}	−45.83
{0 1 $\bar{2}$}	−46.83	{1 0 $\bar{4}$}	−92.11	{0 1 $\bar{2}$}	−48.13
{$\bar{1}$ 0 $\bar{1}$}	−48.88	{0 1 3}	−93.03	{$\bar{1}$ 0 $\bar{2}$}	−51.33
{1 1 0}	−59.15	{1 0 $\bar{2}$}	−93.19	{$\bar{1}$ $\bar{1}$ 0}	−62.12
{$\bar{1}$ 1 $\bar{1}$}	−61.15	{$\bar{1}$ 0 0}	−94.33	{1 1 1}	−64.81
{1 1 $\bar{1}$}	−62.81	{$\bar{1}$ 0 $\bar{2}$}	−95.47	{1 $\bar{1}$ 2}	−68.65
{1 $\bar{1}$ 2}	−63.46	{1 0 4}	−100.47	{$\bar{1}$ 1 $\bar{3}$}	−73.20
{$\bar{1}$ 0 $\bar{3}$}	−65.46	{0 $\bar{1}$ $\bar{4}$}	−102.04		
{1 1 $\bar{2}$}	−67.45	{1 1 1}	−122.02		
{1 $\bar{1}$ 3}	−71.27	{$\bar{1}$ $\bar{1}$ 0}	−123.08		
{$\bar{1}$ 1 $\bar{4}$}	−79.08	{$\bar{1}$ $\bar{1}$ 1}	−125.74		
		{$\bar{1}$ $\bar{1}$ $\bar{2}$}	−126.02		
		{$\bar{1}$ $\bar{1}$ 2}	−128.49		
		{$\bar{1}$ $\bar{1}$ $\bar{3}$}	−130.02		
		{1 $\bar{1}$ $\bar{3}$}	−131.23		
		{1 $\bar{1}$ $\bar{4}$}	−134.41		
		{$\bar{1}$ $\bar{1}$ $\bar{4}$}	−135.09		
		{$\bar{1}$ 1 5}	−138.40		
		{$\bar{1}$ $\bar{1}$ $\bar{5}$}	−140.16		
		{1 $\bar{1}$ $\bar{6}$}	−142.40		
		{$\bar{1}$ $\bar{1}$ $\bar{6}$}	−147.76		
		{1 $\bar{1}$ $\bar{7}$}	−150.50		
		{1 1 7}	−155.37		

played in Fig. 9. As can be seen from the figure the three experimentally observed orientations have the lowest growth rate in the right order $R_{\{0\,0\,2\}} < R_{\{1\,0\,\bar{1}\}} < R_{\{0\,1\,2\}}$. The habit at a relative driving force of $\Delta\mu/kT = 2.4$, the lowest value simulated where the {0 0 2} form shows growth, is displayed in Fig. 10.

The existence of two distinct habits in one single crystallization batch (see Fig. 3) can be explained by the fact that the {0 0 2} orientation grows either via a spiral growth mechanism or via a 2D nucleation mechanism. To test this hypothesis, simulations of the {0 0 2} orientation with a spiral growth mechanism were also performed. This is accomplished by using a dislocation line bounded by two dislocations with opposite Burger's vectors (see also Fig. 11). The height of the Burger's vector is equal to the length of the **c**-axis.

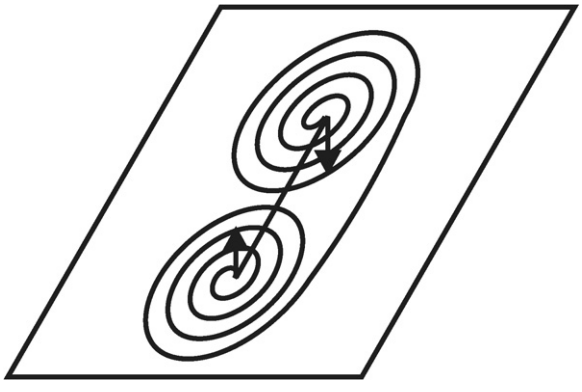

Fig. 11. Spiral growth scheme used in MONTY. Two dislocations with opposite Burger's vector (indicated with arrows) create a dislocation line from which two opposite spirals can grow.

The resulting growth morphology of phase **I**, also at a relative driving force of 2.4, with the {0 0 2} form having a spiral growth mechanism, is displayed in Fig. 12. The morphological importance of the {0 0 2} face is much lower than without a spiral growth mechanism (see Fig. 10) and the {1 0 $\bar{1}$} face becomes dominant, as was also seen experimentally.

For phase **II**, the simulated growth rate as a function of $\Delta\mu/kT$ is displayed in Fig. 13. At $\Delta\mu/kT > 7.0$, the {0 0 2} orientation starts to grow. The morphology at that value for $\Delta\mu/kT$ is displayed in Fig. 14. As can be seen from this figure, when comparing it to the experimental morphology, the predicted morphology is not correct. An octagonal flat crystal is predicted, with the large face being {0 0 2}, and the side faces {1 0 $\bar{4}$}, {1 1 0} and {0 1 1}. Either $R_{1\,0\,\bar{4}}$ or $R_{0\,1\,1}$ is too large, resulting not in a plank-like morphology, but in this octagonal shape.

The high driving force at which phase **II** is predicted to start growing, i.e. $\Delta\mu/kT > 7.0$, hints at the fact that another growth

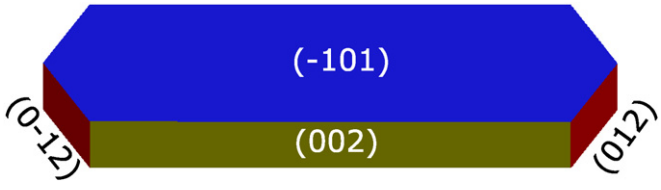

Fig. 12. Predicted morphology at $\Delta\mu/kT = 2.4$ for phase **I** with the {0 0 2} orientation having a spiral growth mechanism.

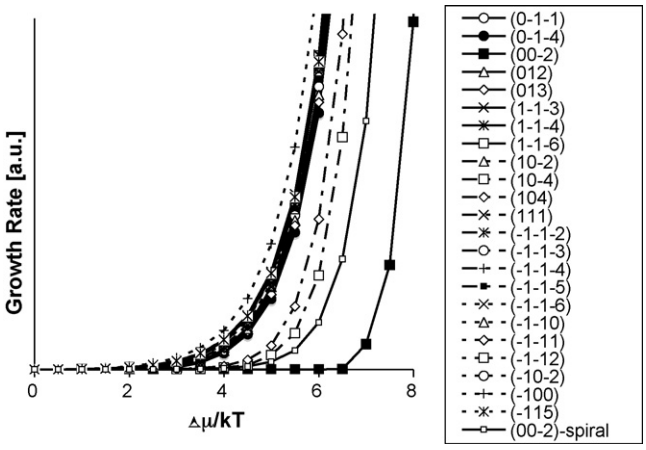

Fig. 13. Monte Carlo growth rate simulations for phase **II**.

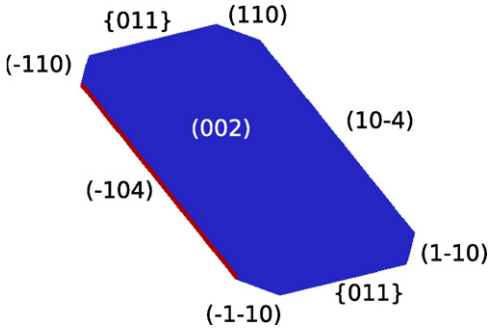

Fig. 14. Predicted morphology for phase **II** at $\Delta\mu/kT = 7.0$.

mechanism may be dominant on the {0 0 2} orientation. To see the effect of spiral growth, simulations were run using a spiral growth mechanism. Using the spiral growth mechanism for phase **II** a more plank-like morphology is predicted at lower driving force value, $\Delta\mu/kT = 4.0$ (see Fig. 15). This shape corresponds better to the experimentally observed morphology. Comparing, however, the orientation of the top faces with the experimentally observed ones (see Fig. 5), the prediction seems

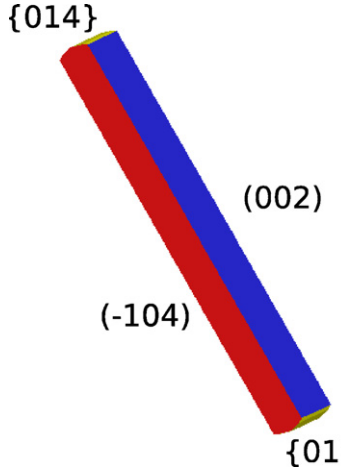

Fig. 15. Predicted morphology at $\Delta\mu/kT = 4.0$ for phase **II** with the {0 0 2} orientation having a spiral growth mechanism. The side faces are {1 0 4} and the top faces are {0 1 4}.

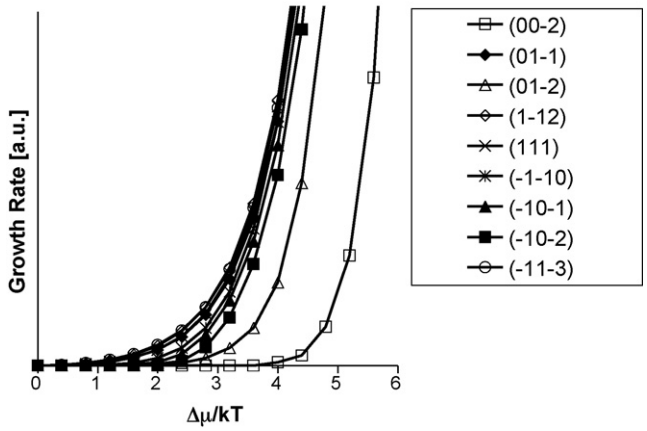

Fig. 16. Monte Carlo growth rate simulations for phase **III**.

to be incorrect. As discussed before, the presence of domains in this phase leading to striations on the top and side faces probably gives rise to ill-defined orientations, which could not be indexed. The growth of these faces is then determined mainly by the domain boundaries acting as step sources, rather than by a 2D nucleation mechanism. Such an effect of domain walls has been observed for, e.g., gibbsite crystals (Sweegers et al., 2004).

The simulated growth rates of phase **III** are displayed in Fig. 16 and the predicted morphology at $\Delta\mu/kT = 4.0$ is displayed in Fig. 17. Although the predicted morphology is quite close to the experimentally observed habit, the predicted indices of the side faces are not correct. The short edges of the rectangle are predicted to be {1 0 1}, but actually they are {0 1 2}, and vice versa. As phase **III** grows as a conglomerate of stacked domains of both enantiomorphs (van Eupen et al., 2008) the relative morphological importance of these two faces might be influenced by that. Face indexation on a goniometer shows that both the conglomerate and the enantiopure crystals have the same indices and morphological importance, in contrast to phase **II**. This is explained by the difference in space group symmetry for the phases: phase **II** has a monoclinic space group ($P12_1/c1$) with its unique axis parallel to the long axis of the crystal. This gives rise to mutually inclined microfacets on the top faces for the twin domains. This, together with the domain boundaries acting as step sources explains the inability to index the crystals of phase **II**. Phase **III**, on the other hand, has an

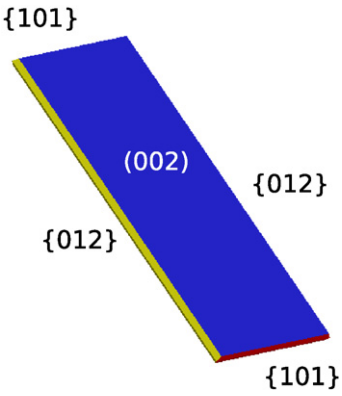

Fig. 17. Predicted morphology for phase **III** at $\Delta\mu/kT = 4.0$.

orthorhombic space group ($P2_12_12_1$) leading to no inclination between the microfacets on the top faces. The presence of the domains, however, can still lead to different growth rates for the top faces, as well as the side faces, compared to the predictions.

6. Conclusions

From the free base form of the anti-depressive drug Venlafaxine, the dominant morphologies of three polymorphs were studied experimentally. Using theories with different levels of complexity, the observed growth morphologies were correlated with the predicted morphologies. For all polymorphs the predicted morphology according to the BFDH theory does not give good results. The Hartman–Perdok theory does better, but fails to predict some indices and – more importantly – fails to predict the rectangular plank-like habits of the polymorphs and instead predicts square plank or cube-like morphologies.

The results of the Monte Carlo growth simulations, which account for both the driving force and the growth mechanism, are very promising. For phase **I** the predictions reproduce the experimentally observed morphology using a 2D nucleation mechanism. A second habit, also observed experimentally, in which $\{\bar{1}\,0\,1\}$ is the dominant face, is found for phase **I** when a spiral growth mechanism is used for the $\{0\,0\,2\}$ orientation.

The simulated growth rate of the $\{0\,0\,2\}$ orientations of phase **II** was very low until high driving forces. Consequently, the predicted morphology did not agree very well with the experimentally observed morphology. When a spiral growth mechanism was used here, the morphology could be predicted at lower $\Delta\mu/kT$ values. This reproduced the experimentally observed morphology more accurately. The observed domains in the crystal structure of phase **II**, interpreted as twin domains, may explain the differences between the morphologies obtained using simulations of 2D nucleation and the observed morphology. The twin domains may act as step sources, facilitating growth at lower driving force.

The simulations of phase **III** also show a rectangular platelike habit, in close correlation with the observed habit. The relative morphological importance of the $\{1\,0\,1\}$ and $\{0\,1\,2\}$ faces is not reproduced however; the $\{1\,0\,1\}$ faces are predicted to be at the short end of the rectangle, whereas the $\{0\,1\,2\}$ faces are experimentally observed to be the short side of the rectangle, and vice versa.

It can thus be concluded that the MONTY simulations are a promising tool for studying crystal growth. Although not all indices of phase **III** could be predicted correctly, all phases did give a semi-quantitative agreement between the experimentally observed habit and the predicted morphology, as far as the overall shape is concerned. The inability of the BFDH method and attachment energy method to predict the morphology correctly for any of the phases shows that the Monte Carlo simulations are a welcome addition to the set of tools for morphology prediction. It is not surprising that when crystals show a more complicated growth behavior than that captured by the mechanisms used by MONTY, e.g. when twinning causes striations and macrosteps, which in turn act as step sources, the simulations no longer show a good agreement with the observed growth behaviour.

Acknowledgement

The authors of the paper would like to acknowledge Dr. W.J.P. van Enckevort for the stimulating and fruitful discussions and help with interpretation of the DICM figures.

References

Boerrigter, S.X.M., Josten, G.P.H., van de Streek, J., Hollander, F.F.A., Los, J., Cuppen, H.M., Bennema, P., Meekes, H., 2004. MONTY: Monte Carlo crystal growth on any crystal structure in any crystallographic orientation: application to fats. J. Phys. Chem. A 108, 5894–5902.

Cerius^2 (1997). Cerius^2 User Guide. Accelrys Inc., San Diego, CA, USA.

Cornell, W.D., Cieplak, P., Bayly, C.I., Kollman, P.A., 1993. Application of RESP charges to calculate conformational energies, hydrogen bond energies and free energies of solvation. J. Am. Chem. Soc. 115, 9620–9631.

Cuppen, H.M., Meekes, H., van Enckevort, W.J.P., Bennema, P., Vlieg, E., 2003. The effects of kink correlation and the Monte Carlo probability scheme on the step structure and velocity. Surf. Sci. 525, 1–12.

Donnay, J.D.H., Harker, G., 1937. A new law of crystal morphology extending the law of bravais. Am. Miner. 22, 446–467.

Donnay, J.D.H., Harker, G., 1961. Assemblage liaisons et structure cristalline. C.R. Acad. Sci. Paris 252, 908–909.

Frisch, M.J., Trucks, G.W., 1995. Gaussian 94 (Revision D.4). Gaussian, Inc., Pittsburgh, PA.

Grimbergen, R., van Hoof, P., Meekes, H., Bennema, P., C-program FACELIFT for connected net analysis, Department of Solid State Chemistry, University of Nijmegen.

Grimbergen, R.F.P., Meekes, H., Bennema, P., Strom, C.S., Vogels, L.J.P., 1998. On the prediction of crystal morphology. I. The Hartman–Perdok theory revisited. Acta Cryst. A 54, 491–500.

Hartman, P., Bennema, P., 1980. The attachment energy as a habit-controlling factor. I. Theoretical considerations. J. Cryst. Growth 49, 145–156.

Hartman, P., Perdok, W., 1955a. On the relations between structure and morphology of crystals. I. Acta Cryst. 8, 49–52.

Hartman, P., Perdok, W., 1955b. On the relations between structure and morphology of crystals. II. Acta Cryst. 8, 521–524.

Hartman, P., Perdok, W., 1955c. On the relations between structure and morphology of crystals. III. Acta Cryst. 8, 525–529.

Husbands, G.E.W., Yardley, J.P., Muth, E.A. Phenylethylamine derivatives and intermediates therefor. Patent EP0112669B1 (1987).

Mayo, S.L., Olafson, B.D., Goddard III, W.A., 1990. Dreiding: a generic force field for molecular simulations. J. Phys. Chem. 94, 8897–8909.

Picha, F., Cucala Escoi, J., Keltjens, R. Venlafaxine base. WO03/082806 and US2003191347 (2003).

Pigache, A., Cieplak, P., Dupradeau, F.-Y., 2004. Automatic and highly reproducible RESP and ESP charge derivation: application to the development of programs RED and X RED. In: Proceedings of the 227th ACS National Meeting, Anaheim, CA, March 28–April 1.

Sweegers, C., Meekes, H., van Enckevort, W.J.P., Hiralal, I.D.K., Rijkeboer, A., 2004. Growth rate analysis of gibbsite single crystals growing from aqueous sodium aluminate solutions. Cryst. Growth Design 4, 185–198.

van der Eerden, J.P., 1993. Handbook of Crystal Growth, Chapter 6. Crystal Growth Mechanisms. North-Holland, Elsevier, Amsterdam, pp. 307.

van Eupen, J.T.H., Elffrink, W., Keltjens, R., Bennema, P., de Gelder, R., Smits, J.M.M., van Eck, E.R.H., Kentgens, A.P.M., Deij, M.A., Meekes, H., Vlieg, E., 2008. Experimental phase diagram of three polymorphs of Venlafaxine base. Cryst. Growth Design 8, in press.

Vippagunta, S.R., Brittain, H.G., Grant, D.J.W., 2001. Crystalline solids. Adv. Drug Deliv. Rev. 48, 3–26.

York, P., 1983. Solid-state properties of powders in the formulation and processing of solid dosage forms. Int. J. Pharm. 14, 1–28.